Cessation of viscoplastic Poiseuille flow with wall slip

CrossMark

Yiolanda Damianou, Maria Philippou, George Kaoullas, Georgios C. Georgiou *

Department of Mathematics and Statistics, University of Cyprus, P.O. Box 20537, 1678 Nicosia, Cyprus

ARTICLE INFO

ABSTRACT

We solve numerically the cessation of axisymmetric Poiseuille flow of a Herschel–Bulkley fluid under the assumption that slip occurs along the wall. The Papanastasiou regularization of the constitutive equation is employed. As for the slip equation, a power-law expression is used to relate the wall shear stress to the slip velocity, assuming that slip occurs only above a critical wall shear stress, known as the slip yield stress. It is shown that, when the latter is zero, the fluid slips at all times, the velocity becomes and remains uniform before complete cessation, and the stopping time is finite only when the slip exponent $s < 1$. In the case of Navier slip ($s = 1$), the stopping time is infinite for any non-zero Bingham number and the volumetric flow rate decays exponentially. When $s > 1$, the decay is much slower. Analytical expressions of the decay of the flat velocity for any value of s and of the stopping time for $s < 1$ are also derived. Using a discontinuous slip equation with slip yield stress poses numerical difficulties even in one dimensional time-dependent flows, since the transition times from slip to no-slip and vice versa are not known a priori. This difficulty is overcome by regularizing the slip equation. The numerical results showed that when the slip yield stress is non-zero, slip ceases at a finite critical time, the velocity becomes flat only in complete cessation, and the stopping times are finite, in agreement with theoretical estimates.

© 2013 Elsevier B.V. All rights reserved.

1. Introduction

If the pressure gradient applied in fully-developed Newtonian Poiseuille flow with no-slip at the wall is suddenly set to zero, the velocity decays to zero exponentially, i.e. the theoretical stopping time is infinite (see, e.g., Ref. [1]). This is not the case for viscoplastic or yield-stress materials [2,3], i.e. materials displaying fluid-like behavior only above a critical stress value, the yield stress τ_0, and solid-like one otherwise. Viscoplastic behavior is exhibited by many structured fluids, such as concentrated suspensions, emulsions, colloidal gels, drilling fluids in petroleum industry, nanocomposites, pastes, cement, granular materials, foodstuffs, and foams [4–6].

The simplest viscoplastic constitutive equation is that of Bingham fluids. In incompressible flow, the stress tensor $\boldsymbol{\tau}$ is given by

$$\begin{cases} \dot{\boldsymbol{\gamma}} = \mathbf{0}, & \tau \leqslant \tau_0 \\ \boldsymbol{\tau} = \left(\frac{\tau_0}{\dot{\gamma}} + \mu\right)\dot{\boldsymbol{\gamma}} & \tau \geqslant \tau_0 \end{cases} \tag{1}$$

where μ is the plastic viscosity,

$$\dot{\boldsymbol{\gamma}} \equiv \nabla \mathbf{u} + (\nabla \mathbf{u})^T \tag{2}$$

is the rate of strain tensor, $\mathbf{u}$ is the velocity vector, and the superscript T denotes the transpose. The magnitudes of $\dot{\boldsymbol{\gamma}}$ and $\boldsymbol{\tau}$, denoted respectively by $\dot{\gamma}$ and τ, are defined by

$$\dot{\gamma} \equiv \sqrt{\frac{1}{2}II_{\dot{\gamma}}} = \sqrt{\frac{1}{2}\dot{\boldsymbol{\gamma}} : \dot{\boldsymbol{\gamma}}} \quad \text{and} \quad \tau \equiv \sqrt{\frac{1}{2}II_{\tau}} = \sqrt{\frac{1}{2}\boldsymbol{\tau} : \boldsymbol{\tau}} \tag{3}$$

where the symbol II stands for the second invariant of a tensor. The Newtonian fluid is recovered by setting $\tau_0 = 0$. The Herschel–Bulkley model is the immediate generalization of the Bingham model:

$$\begin{cases} \dot{\boldsymbol{\gamma}} = \mathbf{0}, & \tau \leqslant \tau_0 \\ \boldsymbol{\tau} = \left(\frac{\tau_0}{\dot{\gamma}} + k\dot{\gamma}^{n-1}\right)\dot{\boldsymbol{\gamma}} & \tau \geqslant \tau_0 \end{cases} \tag{4}$$

where k is the consistency index and n is the power-law exponent. The power-law fluid and the Bingham plastic are special cases of the Herschel–Bulkley fluid, recovered by setting $\tau_0 = 0$ and $n = 1$, respectively.

In any flow of a yield-stress fluid, determination of the yielded ($\tau \geqslant \tau_0$) and unyielded ($\tau \leqslant \tau_0$) regions in the flow field is required, which is not an easy task, especially in two- and three-dimensional problems. To overcome this difficulty several regularized models have been proposed. The most popular regularization in the literature is that proposed by Papanastasiou [7]. The Papanastasiou-regularized version of the Herschel–Bulkley model is:

$$\boldsymbol{\tau} = \left\{ \frac{\tau_0[1 - \exp(-m\,\dot{\gamma})]}{\dot{\gamma}} + k\dot{\gamma}^{n-1} \right\}\dot{\boldsymbol{\gamma}} \tag{5}$$

where m is a stress growth exponent. For sufficiently large values of the regularization parameter m, the Papanastasiou model provides a satisfactory approximation of the Herschel–Bulkley model, while at the same time the need of determining the yielded and the

* Corresponding author. Tel.: +357 22892612; fax: +357 22895352.
E-mail address: georgios@ucy.ac.cy (G.C. Georgiou).

unyielded regions is eliminated. The model has been used with great success in solving various steady and time-dependent flows (see, for example, [8,9] and references therein). Regularization methods may be convenient for engineering calculations of viscoplastic flows, but may fail to describe certain viscoplastic effects and to accurately determine the yield surfaces separating yielded and unyielded regions [10,11]. A better suited alternative is the augmented Lagrangian method (ALM) with an Uzawa-like iteration [12,13]. A critical review of numerical simulations of viscoplastic flow is that of Dean et al. [14].

Theoretical upper bounds of the stopping time of Poiseuille and Couette flows of Bingham plastics have been derived in the case of no wall slip [2,3]. These bounds depend on the density, the plastic viscosity, the yield stress, and the leading eigenvalue of the second-order linear differential operator for the interval under consideration. Also, Huilgol [15] obtained upper bounds of the stopping times in cessation of axisymmetric Poiseuille flows for more general viscoplastic models. These asymptotic bounds are sharp as confirmed by numerical simulations. Chatzimina et al. [10,16] carried out finite element calculations with the regularized Papanastasiou model for Couette and Poiseuille flows of Bingham plastics. The numerical simulations showed in particular that the decay of the volumetric flow rate, which is exponential in the Newtonian case, is accelerated and eventually becomes linear as the yield stress is increased. Zhu and De Kee [17] solved numerically the cessation of plane Couette flow of a regularized yield-stress fluid exhibiting shear thinning and found that the shear thinning parameter increases the stopping time at low and moderate Bingham numbers and has no effect at high ones. Muravleva et al. [12,13] used the augmented Lagrangian method to solve cessation Poiseuille and circular Couette flows. Their results showed that in certain cases the Lagrangian method gives better results that the regularization method, i.e. for the location of the yield surface and the stopping time at low Bingham numbers.

Viscoplastic materials, such as polymeric solutions, suspensions, and gels, are known to exhibit wall slip [18–20]. Denn [21] also noted that wall slip in pasty materials appears within a range of small strains in contrast to the case of polymer melts where slip is observed at large rates of strains. Kalyon [22] analyzed the apparent slip flows of Herschel–Bulkley fluids in various geometries assuming that the apparent slip layer consists solely of the binder and its thickness is independent of the flow rate and the nature of the flow mechanism. He also concluded that the slip (or sliding) velocity, u_w, defined as the relative velocity of the fluid with respect to that of the wall, is related to the wall shear stress, τ_w, by a slip equation of the form

$$\tau_w = \beta u_w^s \qquad (6)$$

where β is the slip coefficient and s is the power-law index of the binder [22]. In the case of Newtonian binders, $s = 1$ and the classical Navier slip condition [23] is recovered. In the case of binders exhibiting a power-law type shear viscosity, $s \neq 1$. It should also be noted that Eq. (6) is a static slip model. Both static and dynamic slip models are discussed by Hatzikiriakos [24]. The slip coefficient depends on the temperature, the normal stress, molecular parameters and on the properties of the fluid/wall interface [21,24]. In the case of fluids with zero yield-stress, the no-slip and plug-flow limiting cases are recovered when $\beta \to \infty$ and $\beta = 0$, respectively. As demonstrated in [25], in the case of yield-stress fluids there is a lower non-zero bound for β at which plug flow is achieved.

In the past thirty years, the power-law slip Eq. (6) has been widely employed by several investigators working on various fluid systems, e.g. by Cohen and Metzner [26], who studied experimentally the occurrence of slip in aqueous and organic polymer solutions, and by Jiang et al. [27] to describe the slip exhibited by gels used in hydraulic fracturing. A power-law relationship

between the slip velocity and the wall shear stress was also predicted at constant temperature by the theoretical model of Lau and Schowalter [28], which was based on the concept of junctions at the wall/polymer interface and in the bulk of the polymer fluid. Eq. (6) has also been used for highly filled suspensions [18] and for polyethylene melts [29–31]. A discussion on the validity of Eq. (7) as well as values of β and s for certain systems are provided by Yilmazer and Kalyon [18]. More recently, Pérez-González et al. [32] carried out two-dimensional particle image velocimetry experiments on a model yield-stress fluid, i.e. a Carbopol gel, which showed that the slip velocity increases in a power-law way with the wall shear stress.

The onset of slip is very often associated with a critical shear stress, called slip yield stress, not only in the case of complex fluids but also in the case of Newtonian liquids under certain conditions. For example, Spikes and Granick [33] reported that for water and tetradecane (which are Newtonian) the slip yield stress may become high for lyophilic wall surfaces. Much earlier, it had been well established that complex fluids, such as polymer melts, pastes, and colloidal suspensions, exhibit macroscopic slip above a critical shear stress [21,34–37]. Nevertheless, according to the slip theory of Brochard-Wyart and de Gennes [38] polymer melts slip no matter how small are the applied shear stresses.

In the present work, a generalized slip model is employed of the form

$$\begin{cases} u_w = 0, & \tau_w \leqslant \tau_c \\ \tau_w = \tau_c + \beta u_w^s, & \tau_w > \tau_c \end{cases} \qquad (7)$$

where τ_c is the slip yield stress, which is also called sliding or interfacial or apparent yield stress or friction stress [39]. The above equation, which looks very much like the Herschel–Bulkley plastic constitutive equation, can be viewed as a restricted Coulomb-type friction condition. The term slip "yield stress" was introduced by Durbin [40] in order to alleviate the singularity at a moving contact line. He applied this boundary condition to the flow of a slender Newtonian drop rolling down an incline, concluding that the length of the slip region is a property of the fluid flow. Nevertheless, it should also be noted that the proposed slip model was not discontinuous but smooth (regularized) [40]. Le Roux and Tani [41] refer to slip equations involving slip yield stress as "threshold" slip equations while Piau [42] calls them "friction relations". Roquet and Saramito [43] also used the term "yield-force" for this critical value.

The linear version of Eq. (7), obtained by setting $s = 1$, was first used by Fortin et al. [44] to describe the experimental data of Ramamurthy [34] on a LLDPE in a capillary tube. They calculated τ_c to be 0.0719 MPa. In their sliding-plate experiments on high density polyethylenes, Hatzikiriakos and Dealy [36] used the following simplified (but discontinuous) variant of Eq. (7)

$$\begin{cases} u_w = 0, & \tau_w \leqslant \tau_c \\ \tau_w = \beta u_w^s, & \tau_w > \tau_c \end{cases} \qquad (8)$$

The critical wall shear stress for the onset of slip was found to be 0.09 MPa in both steady and transient experiments. This critical value was reduced to 0.025 MPa when the wall was treated with a certain fluorocarbon but remained unchanged when another fluorocarbon was used. In capillary flow experiments with metallocene polyethylenes, Hatzikiriakos and Kazatchkov [45] found that slip appears for wall shear stresses in the range 0.05–0.1 MPa while Kalyon and Gevgilili [37] measured the slip yield stresses of PDMS and a HDPE to be 0.073 MPa and 0.22 MPa, respectively, and independent of temperature.

The yield stress values reported for other materials, such as Carbopol gels, microgel pastes and some Newtonian fluids are much smaller than those of polymer melts. Piau [42] used Eq. (7) to fit experimental data on Carbopol dispersions at various

concentrations for different wall materials. The values of τ_c for these viscoplastic fluids ranged from 0.2 to 33 Pa while s ranged from about 0.3 to unity. Piau [42] noted that increasing surface roughness tends to increase the slip yield stress at very low slip velocities and the exponent s at high slip velocities. Moreover, s is close to unity for the smoothest surfaces and in the range 0.37–0.5 for some rougher surfaces. From their experimental data on microgel pastes, Seth et al. [46] calculated τ_c in the range 1.25–5.5 Pa and s in the range 0.5–0.65. The linear version of Eq. (7) was also proposed by Spikes and Granick [33] for Newtonian flow. In their model, slip was assumed to occur only if the wall shear stress exceeds τ_c and once slip occurs it takes place at a constant slip length. Their work showed that τ_c is quite small, in the 0.1–2 Pa range for the lyophobic surfaces examined and about 6 Pa for a lyophilic surface. Choo et al. [47] demonstrated that this model can explain data from different experiments on Newtonian fluids. The same expression (with $s = 1$) was employed by Ballesta et al. [20,48] in their experimental study of hard-sphere colloidal suspensions. The latter authors noted that the term βu_w is a hydrodynamic term reflecting the lubrication between the first layer of colloids at the wall.

Hatzikiriakos [49] also adapted Eyring's theory of liquid viscosity to polymer molecules at a solid interface and derived a model which gives the slip velocity as a function of the wall shear stress, the temperature, and molecular parameters. This can be written in the following simplified form

$$u_w = \begin{cases} 0, & \tau_w \leqslant \tau_c \\ u(T) \sinh\left[\frac{E}{RT}\left(\frac{\tau_w}{\tau_c} - 1\right)\right], & \tau_w > \tau_c \end{cases} \tag{9}$$

where T is temperature, R is the molar gas constant, and E represents the minimum amount of energy that the shear stress at the interface has to overcome for slip to occur. The non-monotonic slip equations proposed by Piau and El Kissi [50] for highly entangled polymers and by Leonov [51] for elastomers also include a critical stress threshold below which no slip occurs. Tang and Kalyon [52,53] used a sophisticated slip equation with slip yield stress for their analysis of flow instabilities of polymeric fluids and suspensions. In the present notation this can be written as follows:

$$u_w = \frac{1}{2\beta}\tau_w^{1/s}[1 + \tanh(\alpha(\tau_w - \tau_c))] \tag{10}$$

where β and s are the slip coefficient and the slip exponent of the polymeric binder and α is a positive constant (typically 1-20) describing the sharpness of the weak-to-strong slip transition at $\tau_w = \tau_c$. It should be noted that Eq. (10) yields a (practically) zero slip velocity for $\tau_w < \tau_c$, i.e. there is no need to specify the no-slip boundary condition for $\tau_w < \tau_c$."

In a pioneering paper, Pearson and Petrie [54] proposed the linear version of Eq. (7) for a Bingham fluid, assuming that $\tau_c = \tau_0$. In general, however, the slip yield stress τ_c may be smaller or greater than the bulk yield stress τ_0 depending on the material (affecting both τ_c and τ_0) and the fluid/wall interface (affecting only τ_c). Kalyon [22] pointed out that wall slip is inevitable during the flow of viscoplastic fluids under stress magnitudes that are smaller than their yield stress values, i.e. $\tau_c < \tau_0$. This was also the case with the experiments of Pérez-González et al. [32] on a Carbopol gel. According to Métivier and Magnin [55], experiments on certain concentrated dispersions show that τ_c is smaller than τ_0. However, this is not true with other systems, e.g. for hard-sphere colloidal suspensions in which $\tau_c \geqslant \tau_0$ [20,48]. It should also be mentioned here that certain classes of materials exhibit slip only at low shear stresses, i.e. the slip they exhibit is negligible beyond a critical shear stress. In their review paper, Nguyen and Boger [4] reported that slip is reduced or disappears after yielding. This was also the case with a foam and a model concentrated emulsion used by

Bertola et al. [5] in a series of rheometrical tests. Meeker et al. [56] reported experimental results on microgel pastes and concentrated suspensions showing that slip is negligible compared to the bulk flow, well above the yield stress. These authors noted that slip prevails at and below the yield stress with the bulk flow being negligible; at and just above the yield stress both slip and bulk flows are important. In the experiments of Piau [42] on Carbopol dispersions at different concentrations and wall materials, the calculated values of τ_c were always much (and very often one or two magnitudes) smaller than those of τ_0.

Seth et al. [46] also reported that the slip yield stress is much lower (about an order of magnitude) than τ_0 in the case of concentrated suspensions of soft deformable particles, e.g. polymer microgel pastes and compressed emulsions. They also noted that, when the fluid/wall interactions are attractive, slip yield stress is comparable to the bulk yield stress and the slip velocity increases with the square of the stress (i.e. $s \approx 0.5$) according to data obtained mostly in the plug flow region ($\tau_w < \tau_0$). In the repulsive case, however, the slip yield stress is very low (compared to the bulk yield stress) and the slip velocity is proportional to the applied stress (i.e., $s \approx 1$).

Le Roux and Tani [41] established the wellposedness of steady-state Navier–Stokes equations in bounded domains for the case of boundary conditions with slip yield stress. They also proved the uniqueness of the solution and its continuous dependence on the data. Huilgol [57] extended the variational principles for the Poiseuille flow of a yield stress fluid to include wall slip described by Eq. (7). Analytical solutions of steady both Newtonian and non-Newtonian flows with wall slip following Eq. (7) have also been reported. Fortin et al. [44] considered briefly the steady-state Poiseuille flow of a Bingham plastic and obtained analytical as well as numerical solutions with the augmented Lagrangian method. Métivier and Magnin [55] investigated the effect of wall slip on the stability of the Rayleigh-Bénard plane Poiseuille flow of Bingham plastics (with non-zero slip yield stress). Ballesta et al. [20] derived steady-state solutions for the flow of concentrated colloidal suspensions obeying the Herschel–Bulkley model in a cone-plate geometry. Spikes [58] and, more recently, Tauviqirrahman et al. [59] employed a slip model with slip yield stress to modify the (Newtonian) Reynolds equation in their studies of lubricated parallel sliding contacts.

Analytical steady-state solutions of various Newtonian Poiseuille flows in one- and two-dimensions, including tubes of rectangular [60] and triangular [61] cross-sections have also been reported recently. In one-dimensional flows slip occurs only if the imposed pressure gradient exceeds a critical value. In two-dimensional flows, it is easily seen that slip is triggered in the middle of boundary segments at a critical value of the imposed pressure gradient and may spread everywhere in that segment above a second critical value of the pressure gradient. More recently, Kaoullas and Georgiou [62] derived solutions for various start-up Newtonian Poiseuille flows noting that the classical start-up, no-slip solution holds if the imposed pressure gradient is below the critical value. Otherwise, flow starts without slip up to a critical time at which $\tau_w = \tau_c$ and slip does occur following the second branch of Eq. (7). Obviously, in the case of cessation, the opposite phenomenon is observed: slip occurs only initially up to a critical time such that $\tau_w = \tau_c$ and then flow ceases without wall slip.

The objectives of the present work are to study the cessation of the axisymmetric Poiseuille flow of Herschel–Bulkley fluids with wall slip and to investigate the evolution of yielded/unyielded regions. As already mentioned, solving viscoplastic flows in tubes is of great importance in food and petroleum industries, in ceramics and semi-solid materials processing and in concrete pumping. The regularized version of the constitutive equation is employed in the numerical calculations. A particular feature of such a flow when

slip Eq. (7) is used is the transition of the time-dependent flow from slip to no-slip at a critical time at which τ_w becomes equal to τ_c. Using the discontinuous slip model of Eq. (7) poses difficulties similar to those resulting from the use of the ideal Herschel–Bulkley model, given that the time for the above transition is unknown. To overcome this difficulty we also regularize the slip equation. Hence, in the numerical time-dependent simulations we use the following regularized version of Eq. (7):

$$\tau_w = \tau_c[1 - \exp(-m_c u_w)] + \beta u_w^s \tag{11}$$

where m_c is a growth parameter similar to the stress growth exponent of the Papanastasiou equation. For sufficiently large values of m_c, Eq. (11) is a satisfactory approximation of Eq. (7).

The governing equations are presented and non-dimensionalized in Section 2. The steady-state solutions corresponding to the slip Eq. (7) are derived in Section 3. The different flow regimes, depending on the value of the imposed gradient and the relative values of τ_0 and τ_c, are identified. It is also shown that in the case of non-uniform flow with wall slip there is a lower bound for the admissible value of the slip coefficient which is proportional to $(\tau_0 - \tau_c)$. In Section 4, the analytical time-dependent solutions in the case of a Newtonian fluid ($\tau_0 = 0$, $n = 1$) and a linear slip equation ($s = 1$) are derived. The equation satisfied by the critical time for the slip/no-slip transition is also derived. An approximate explicit formula is also obtained for this critical time. In Section 5, numerical time-dependent solutions are presented for a Bingham fluid and various values of the exponent s. It is shown that if the slip yield stress is zero, the fluid slips at all times and the velocity becomes flat, i.e. the fluid becomes fully unyielded, at a finite time bounded by the estimates of Glowinski [2] and Huilgol et al. [3] and remains so thereafter decaying to zero. An analytical expression for the velocity in this regime has been obtained. It turns out that when the slip yield stress is zero, the stopping time is infinite for $s \geqslant 1$ and finite for $s < 1$. The applicability of the regularized slip Eq. (11) when the slip yield stress is non-zero is checked and the effect of the growth parameter is investigated. In this case, the flow stops in a finite time for any value of the power-law exponent s and the velocity becomes flat only at complete cessation.

2. Governing equations

We consider the laminar pressure-driven flow of a Herschel–Bulkley fluid in a tube of radius R, as shown in Fig. 1. Under the assumptions of unidirectionality and zero gravity, the velocity $u_z(r, t)$ satisfies the continuity equation automatically and the z-momentum equation for any fluid becomes

$$\rho \frac{\partial u_z}{\partial t} = -\frac{\partial p}{\partial z} + \frac{1}{r}\frac{\partial}{\partial r}(r\tau_{rz}) \tag{12}$$

where ρ is the density. The constitutive equation of the material is simplified as follows:

$$\begin{cases} \frac{\partial u_z}{\partial r} = 0, & |\tau_{rz}| \leqslant \tau_0 \\ \tau_{rz} = -\tau_0 - k\left(-\frac{\partial u_z}{\partial r}\right)^n, & |\tau_{rz}| \geqslant \tau_0 \end{cases} \tag{13}$$
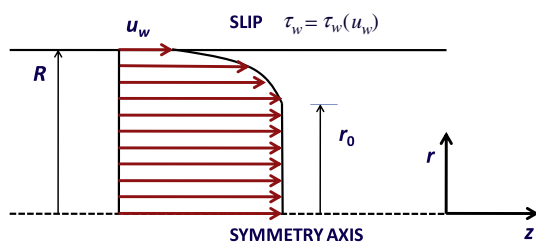

Fig. 1. Axisymmetric Poiseuille flow of a Herschel–Bulkley fluid.

where τ_{rz} is the shear stress and u_z is the axial velocity.

To non-dimensionalize the governing equations we scale lengths by the tube radius, R, the velocity by the mean steady-state velocity, V, the pressure and the stress components by kV^n/R^n, and time by $\rho R^{n+1}/(kV^{n-1})$. With these scalings the dimensionless forms of Eqs. (12) and (13) are as follows:

$$\frac{\partial u_z}{\partial t} = G + \frac{1}{r}\frac{\partial}{\partial r}(r\tau_{rz}) \tag{14}$$

and

$$\begin{cases} \frac{\partial u_z}{\partial r} = 0, & |\tau_{rz}| \leqslant Bn \\ \tau_{rz} = -Bn - \left(-\frac{\partial u_z}{\partial r}\right)^n, & |\tau_{rz}| \geqslant Bn \end{cases} \tag{15}$$

where all variables are now dimensionless (denoted by the same symbols for simplicity),

$$Bn \equiv \frac{\tau_0 R^n}{kV^n} \tag{16}$$

is the Bingham number, and G is the dimensionless pressure gradient.

The dimensionless form of the slip Eq. (7) is

$$\begin{cases} u_w = 0, & \tau_w \leqslant B_c \\ \tau_w = B_c + B u_w^s, & \tau_w > B_c \end{cases} \tag{17}$$

where

$$B \equiv \frac{\beta R^n V^{s-n}}{k} \tag{18}$$

is the usual slip number and

$$B_c \equiv \frac{\tau_c R^n}{kV^n} \tag{19}$$

is the slip yield stress number. The no-slip condition corresponds to $B \to \infty$. The full-slip limiting case is recovered when $B = 0$ for a Newtonian fluid and at a finite value of B for a yield stress fluid, as discussed below. In the special case $\tau_c = \tau_0$, the slip yield stress and the Bingham numbers are identical.

3. Steady-state Herschel–Bulkley flows with slip

The solution of the steady, incompressible Poiseuille flow of a Herschel–Bulkley fluid in the special case of Navier slip ($B_c = 0$, $s = 1$) has been provided under different forms by Kalyon et al. [63]. Taking into account the slip yield stress and noting that in steady-state the dimensionless wall shear stress for any generalized Newtonian fluid is $\tau_w = G/2$, we can identify four different possibilities depending on the value of the applied pressure gradient, G, and the relative values of B_c and Bn. These possibilities, also illustrated in Fig. 2, are the following:

(i) If $G \leqslant \min\{2B_c, 2Bn\}$, then no flow occurs. (In this case, the velocity scale V used for the non-dimensionalization is an arbitrary, non-zero velocity.)
(ii) If $G \geqslant \max\{2B_c, 2Bn\}$, then we have non-uniform flow with wall slip and yielded/unyielded regions in the flow domain. The dimensionless velocity profile is given by

$$u_z(r) = u_w + \frac{n}{2^{1/n}(n+1)} G^{1/n} \begin{cases} (1-r_0)^{1/n+1}, & 0 \leqslant r \leqslant r_0 \\ [(1-r_0)^{1/n+1} - (r-r_0)^{1/n+1}], & r_0 \leqslant r \leqslant 1 \end{cases} \tag{20}$$

where

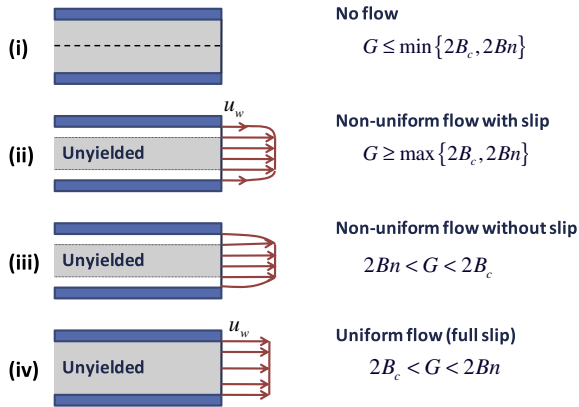$$u_w = \left(\frac{G - 2B_c}{2B}\right)^{1/s} \tag{21}$$

Fig. 2. Different possibilities in Poiseuille flow of a Herschel–Bulkley fluid depending on the imposed dimensionless pressure gradient, G, and the values of the slip yield stress number, B_c, and the Bingham number, Bn.

and

$$r_0 = \frac{2Bn}{G} \leqslant 1 \qquad (22)$$

is the yield point. The dimensionless pressure-gradient is a solution of the following equation:

$$2^{1/n} \frac{3n+1}{n} (1 - u_w) G^3 = (G - 2Bn)^{1/n+1}$$
$$\times \left[G^2 + \frac{4nBn}{2n+1} G + \frac{8n^2 Bn^2}{(n+1)(2n+1)} \right] \qquad (23)$$

(iii) If $2Bn < G < 2B_c$, then the fluid flows without slip ($u_w = 0$) with distinct yielded and unyielded regions. Eqs. (20) and (23) still apply.

(iv) Finally, if $2B_c < G < 2Bn$, the fluid is unyielded everywhere in the flow domain, translating with unit velocity as a rigid body (the motion is entirely due to wall slip).

It is clear that the sequence of the flow regimes as the pressure gradient is increased is $(i) \rightarrow (iv) \rightarrow (ii)$ if $Bn > B_c$, $(i) \rightarrow (iii) \rightarrow (ii)$ if $B_c < Bn$, and $(i) \rightarrow (ii)$ if $B_c = Bn$. As already mentioned, the existence of regime (iv) where the flow results solely from wall slip while the bulk material remains undeformed is characterized as inevitable by Kalyon [22]. This regime has been observed directly by means of nuclear magnetic resonance on different yield-stress materials, such as tomato sauce, egg white, and concentrated suspensions (see [5] and references therein). It is also clear how slip may obscure the viscoplastic nature of the material, since the apparent flow due to slip hides the yield stress behavior [39]. Lindner et al. [64] noted that the yield stress of a foam they investigated was revealed only when the boundaries were modified to inhibit slip. According to Sochi [39], because the local stress in this regime is below the yield stress except possibly at the boundary region, no yielding occurs except at a very thin layer adjacent to the surface, which serves as a lubricating thin film. Other explanations include the formation of a depleted inhomogeneous layer from the continuum phase where sliding occurs, or through a film which exists on the wall prior to the experiment or generated from the bulk phase [4,39]. Purely plug flow profiles in regime (iv) (i.e. before yielding) have also been observed in the experiments of Seth et al. [46] on microgel pastes and, more recently, in those of Pérez-González et al. [32] on a Carbopol gel. These authors also reported that the slip velocity increases even further after yielding (i.e. in regime (ii)). These observations, however, disagree with previous works mostly on concentrated suspensions where the reduction and almost the disappearance of the slip velocity had been observed

after yielding [4]. Slip in such systems was attributed to the formation of a liquid film adjacent to the wall acting as a lubricant, the effect of which is reduced at higher shear stresses or by using tubes with rough walls [4].

When no-slip is applied, r_0 tends to unity asymptotically as Bn goes to infinity. Otherwise, it is deduced from Eq. (23) that a flat velocity profile ($u_x = u_w = 1$) is attained when $G = 2Bn > 2B_c$. In the Newtonian case ($Bn = 0$), the velocity tends to a plug profile ($u_x = u_w = 1$) in the limit of zero B (perfect slip). Interestingly, with viscoplastic fluids, the yield distance r_0 tends to unity and thus the velocity tends to become plug as B approaches a finite non-zero value, B_{crit}. From Eqs. (21) and (22) one finds:

$$B_{crit} = Bn - B_c \qquad (24)$$

Hence, for given Bn and B_c, solutions for slip numbers below or equal to B_{crit} are not admissible. Similarly, when B and B_c are given, there exists a critical upper bound for the Bingham number, $Bn_{crit} = B + B_c$, which cannot be exceeded. At Bn_{crit} both the yield distance and the slip velocity become 1. This implies that the flow becomes plug at a critical wall shear stress, which is consistent with experimental observations on highly filled suspensions [18].

The pressure gradient corresponding to the no-slip case sets an upper bound G_{max} for G. This can be determined from Eq. (23) after setting u_w to zero. From Eq. (21) it is deduced that the upper bound for the admissible values of B_c is

$$B_{c,max} = \frac{1}{2} G_{max} \qquad (25)$$

In the case of a power-law fluid one finds that

$$u_z(r) = u_w + \frac{3n+1}{n+1} (1 - u_w)(1 - r^{1/n+1}) \qquad (26)$$

and

$$G = 2 \left(3 + \frac{1}{n} \right)^n (1 - u_w)^n \qquad (27)$$

where the slip velocity is the solution of

$$u_w = \left\{ \frac{1}{B} \left[\left(3 + \frac{1}{n} \right)^n (1 - u_w)^n - B_c \right] \right\}^{1/s} \qquad (28)$$

Therefore, $B_{c,max}$ is independent of the slip exponent s:

$$B_{c,max} = \left(3 + \frac{1}{n} \right)^n \qquad (29)$$

In the general case, Eq. (28) for u_w is solved numerically. In the case of Newtonian flow with $s = 1$, one finds that

$$u_w = \frac{4 - B_c}{B + 4} \qquad (30)$$

and

$$u_z(r) = \frac{4 - B_c}{B + 4} + 2 \frac{B + B_c}{B + 4} (1 - r^2) \qquad (31)$$

It is clear that $B_{c,max} = 4$. Other solutions of (28) for selected values of n and s are provided in Table 1.

The case of Herschel–Bulkley flow with Navier slip ($B_c = 0$ and $s = 1$) has been discussed in detail by Damianou et al. [25], where, however, a different definition of the slip number was employed (A_1 in their paper corresponds to $1/(2B)$). Here we first consider Bingham flow ($n = 1$) with zero slip yield stress ($B_c = 0$). In such a case, the pressure gradient G is a root of

$$24 \left(\frac{G}{2B} \right)^{1/s} G^3 + 3G^4 - 8(Bn + 3)G^3 + 16Bn^4 = 0 \qquad (32)$$

Table 1
Dimensionless pressure gradient and slip velocity for a power-law fluid for different values of the exponents n and s.

n	s	Pressure gradient	Slip velocity
1	1	$G = \frac{8(B+B_c)}{B+4}$	$u_w = \frac{4-B_c}{B+4}$
	2	$G = 8(1-u_w)$	$u_w = \frac{2}{B}\left(\sqrt{1+\frac{B}{4}(4-B_c)}-1\right)$
	1/2		$u_w = \frac{1}{64}\left(\sqrt{B^2+16(4-B_c)}-B\right)^2$
1/2	1	$G = \sqrt{20(1-u_w)}$	$u_w = \frac{-(2BB_c+5)+\sqrt{(2BB_c+5)^2+4B^2(5-B_c^2)}}{2B^2}$
	1/2		$u_w = \frac{\left[-2BB_c+\sqrt{4B^2B_c^2+4(B^2+5)(5-B_c^2)}\right]^2}{4(B^2+5)^2}$
2	1	$G = \frac{49}{2}(1-u_w)^2$	$u_w = \left(1+\frac{2B}{49}\right)\left[1-\sqrt{1-\frac{1-\frac{48c}{49}}{\left(1+\frac{2B}{49}\right)^2}}\right]$

The effect of the exponent s when B_c is still zero is illustrated in Figs. 3 and 4, which show velocity profiles for $s = 1/2$, 1 and 2, $n = 1$, various slip numbers, and $Bn=0$ and 1, respectively. In the latter case (Bingham flow), the velocity becomes flat at the critical slip number $B_{crit} = Bn$.

Let us now focus on the special case when $Bn = B_c$, in which only the flow regimes (i) and (ii) are possible. In other words, slip and deformation occur simultaneously and there are no bounds for the slip and Bingham numbers. For simplicity, we restrict ourselves to the Bingham-plastic case ($n = 1$), in which the dimensionless pressure gradient G is a root of

$$24\left(\frac{G-2Bn}{2B}\right)^{1/s}G^3 + 3G^4 - 8(Bn+3)G^3 + 16Bn^4 = 0 \qquad (33)$$
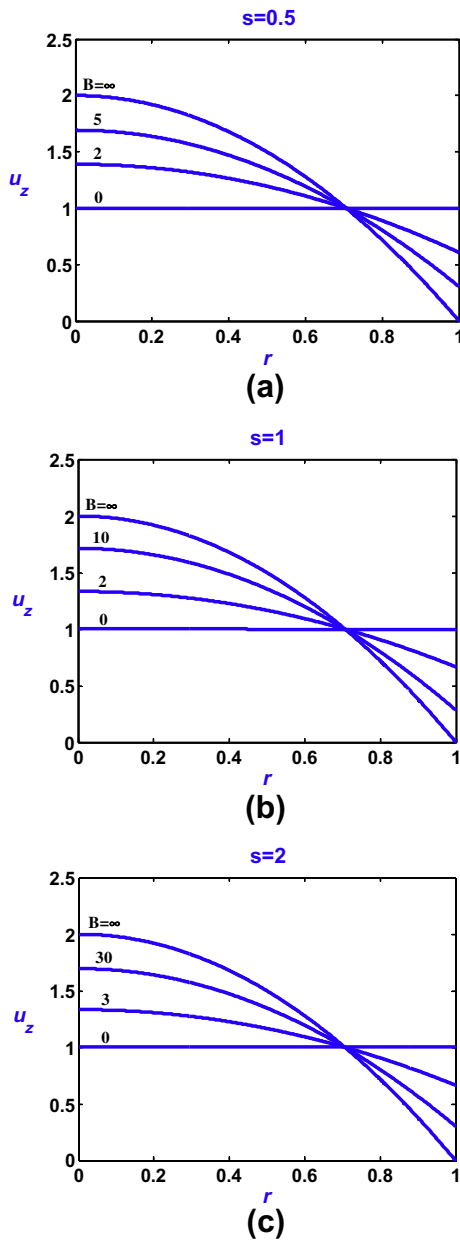
Fig. 3. Steady velocity profiles in axisymmetric Poiseuille flow of a Newtonian fluid ($Bn = 0$) with zero slip yield stress ($B_c = 0$) and different values of the slip number: (a) $s = 0.5$; (b) $s = 1$; and (c) $s = 2$.
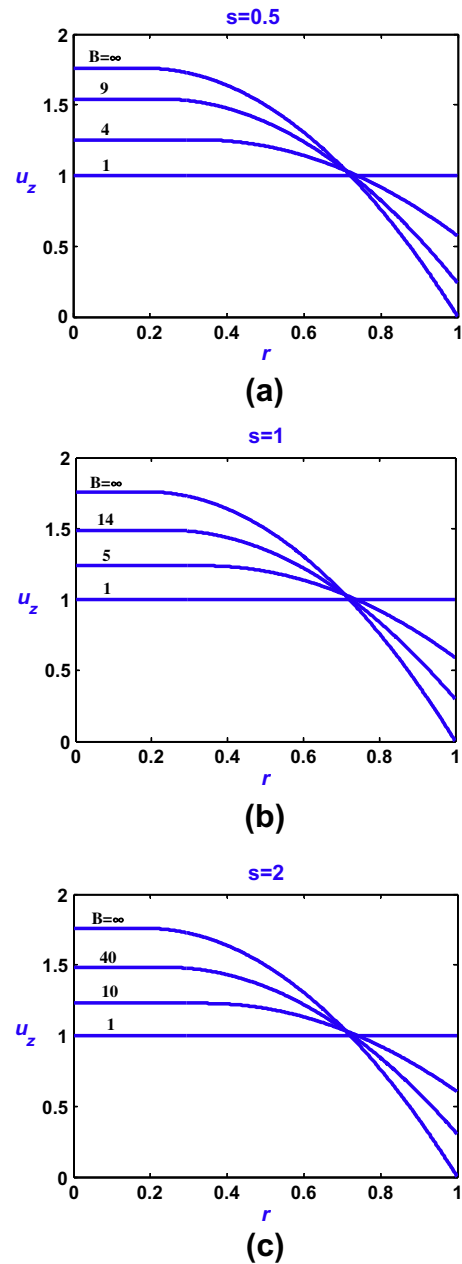
Fig. 4. Steady velocity profiles in axisymmetric Poiseuille flow of a Bingham plastic ($Bn = 1$) with zero slip yield stress ($B_c = 0$) and different values of the slip number: (a) $s = 0.5$; (b) $s = 1$; and (c) $s = 2$.
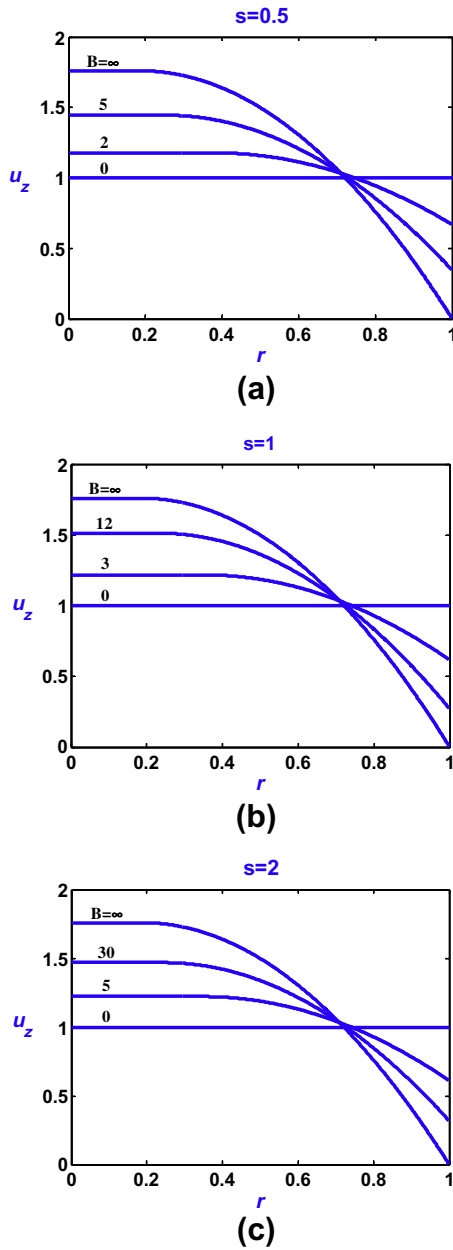
Fig. 5. Steady velocity profiles in axisymmetric Poiseuille flow of a Bingham plastic with $Bn = B_c = 1$ and different values of the slip number: (a) $s = 0.5$; (b) $s = 1$; and (c) $s = 2$.
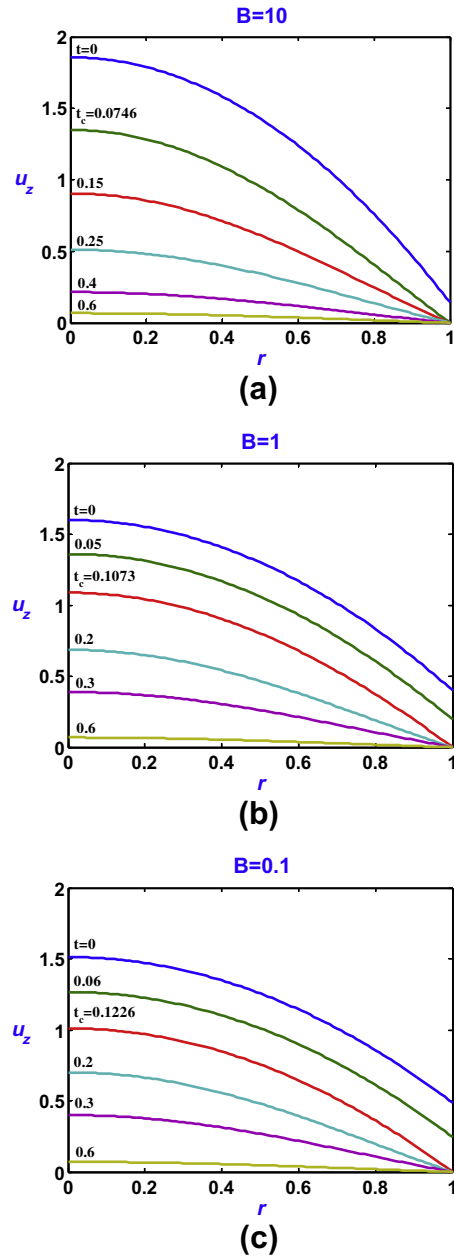

Fig. 6. Evolution of the velocity in cessation of axisymmetric Poiseuille flow of a Newtonian fluid with $B_c = 2$ and $s = 1$: (a) $B = 10$; (b) $B = 1$; and (c) $B = 0.1$.

The results for $Bn = B_c = 0$ are those shown in Fig. 3 (Newtonian flow with zero slip yield stress). The effect of the exponent s for $Bn = B_c = 1$ is illustrated in Fig. 5. Comparing these results to those of Fig. 4 (zero B_c) we observe that similar changes in the velocity profile are observed at lower values of B and the critical value of the slip number for the velocity to become flat is $B_{crit} = 0$.

4. Cessation of Newtonian flow with non-zero slip yield stress

Consider the cessation of Newtonian flow with non-zero slip yield stress in the special case that $s = 1$, so that the problem is amenable to analytical solution. The dimensionless z-momentum equation takes the form

$$\frac{\partial u_z}{\partial t} = G + \frac{\partial^2 u_z}{\partial r^2} + \frac{1}{r}\frac{\partial u_z}{\partial r} \qquad (34)$$

The wall boundary condition may be written as follows:

$$u_w = \begin{cases} 0, & \tau_w \leqslant B_c \\ \frac{1}{B}(\tau_w - B_c), & \tau_w > B_c \end{cases} \qquad (35)$$

where

$$\tau_w = -\frac{\partial u_z}{\partial r}\bigg|_{r=1} \qquad (36)$$

The steady-state velocity is thus given by

$$u_z(r) = \begin{cases} 2(1 - r^2), & G \leqslant 2B_c \\ \frac{4 - B_c}{B + 4} + 2\frac{B + B_c}{B + 4}(1 - r^2), & G > 2B_c \end{cases} \qquad (37)$$

For the time-dependent calculations, we assume that at $t = 0$ the velocity $u_z(r, t)$ is given by the steady-state solution (37) and that at $t = 0^+$ the steady-state pressure gradient G is set to zero. If

$G \leqslant 2B_c$, then the fluid sticks at the wall at all times and the standard no-slip solution holds:

$$u_z(r,t) = 16 \sum_{k=1}^{\infty} \frac{1}{\lambda_k^3 J_1(\lambda_k)} J_0(\lambda_k r) e^{-\lambda_k^2 t} \tag{38}$$

where λ_k are the roots of J_0. The volumetric flow rate is

$$Q(t) = 32 \sum_{k=1}^{\infty} \frac{1}{\lambda_k^4} e^{-\lambda_k^2 t} \tag{39}$$

If now $G > 2B_c$, slip occurs only initially and the velocity is given by

$$u_z(r,t) = \frac{16(B+B_c)}{B+4} \sum_{k=1}^{\infty} \frac{1}{\alpha_k^3 J_1(\alpha_k)\left(1+\alpha_k^2/B^2\right)} J_0(\alpha_k r) e^{-\alpha_k^2 t} - \frac{B_c}{B} \tag{40}$$

where α_k are the roots of

$$J_0(\alpha_k) - \frac{\alpha_k}{B} J_1(\alpha_k) = 0 \tag{41}$$

It is easily deduced that at the critical time t_c such that

$$\tau_w(t_c) = \frac{16(B+B_c)}{B+4} \sum_{k=1}^{\infty} \frac{1}{\alpha_k^2\left(1+\alpha_k^2/B^2\right)} e^{-\alpha_k^2 t_c} = B_c \tag{42}$$

slip ceases and the no-slip condition is applied (Eq. (42) is equivalent to $u_z(1,t_c) = 0$). For $t > t_c$, the velocity is given by

$$u_z(r,t) = 2 \sum_{n=1}^{\infty} \frac{1}{\lambda_n B J_1(\lambda_n)} \left[\frac{16\lambda_n^2(B+B_c)}{(B+4)} \right.$$
$$\left. \times \sum_{k=1}^{\infty} \frac{1}{\alpha_k^2\left(1+\alpha_k^2/B^2\right)(\lambda_n^2-\alpha_k^2)} e^{-\alpha_k^2 t_c} - B_c \right] J_0(\lambda_n r) e^{-\lambda_n^2(t-t_c)} \tag{43}$$

It should be noted that the eigenvalues λ_n and α_k do not coincide, given that J_0 and J_1 do not have common roots. For the volumetric flow rate one finds that

$$Q(t) = \begin{cases} \frac{32(B+B_c)}{B+4} \sum_{k=1}^{\infty} \frac{1}{\alpha_k^4\left(1+\alpha_k^2/B^2\right)} e^{-\alpha_k^2 t} - \frac{B_c}{B}, & t \leqslant t_c \\ 4\sum_{n=1}^{\infty} \frac{1}{\lambda_n^2 B}\left[\frac{16\lambda_n^2(B+B_c)}{(B+4)} \sum_{k=1}^{\infty} \frac{1}{\alpha_k^2\left(1+\alpha_k^2/B^2\right)(\lambda_n^2-\alpha_k^2)} e^{-\alpha_k^2 t_c} - B_c \right] e^{-\lambda_n^2(t-t_c)}, & t > t_c \end{cases}$$
$$\tag{44}$$

In Fig. 6, we show the evolution of the velocity for different slip numbers ($B = 10$, 1, and 0.1) and $B_c = 2$ (recall that in Newtonian flow, $B_{c,max} = 4$). The profiles at the critical time t_c at which the slip velocity vanishes are also provided in all cases. It should be noted that cessation is slower when slip is stronger, and thus t_c increases

as the slip number B is reduced. This is also illustrated in Fig. 7, where the critical times for $B_c = 1$, 2, and 3 are plotted versus B. A simple lower estimate for t_c can be obtained by considering only the leading term of expansion (42). It turns out that

$$t_c \approx \frac{1}{\alpha_1^2} \ln \frac{16(B+B_c)}{\alpha_1^2\left(1+\alpha_1^2/B^2\right)(B+4)B_c} \tag{45}$$

It can be seen in Fig. 7 that this estimate is quite satisfactory for small values of B_c and improves as B is reduced (i.e., as slip becomes stronger). The evolution of the volumetric flow rate for $B_c = 1$, 2, and 3 and various slip numbers is shown in Fig. 8. Similarly, in Fig. 9 the evolution of the slip velocity and its sudden cessation at t_c is demonstrated for $B_c = 1$, 2, and 3 and various values of B. As already noted, the stronger the slip the slower the cessation is. Our
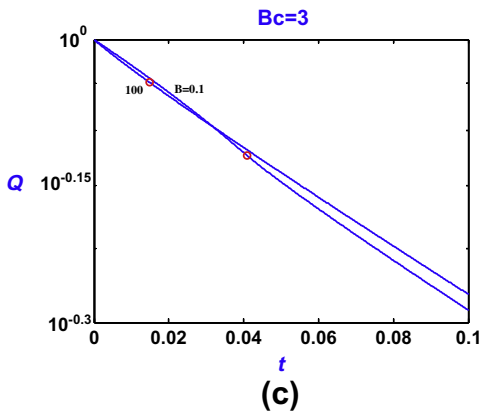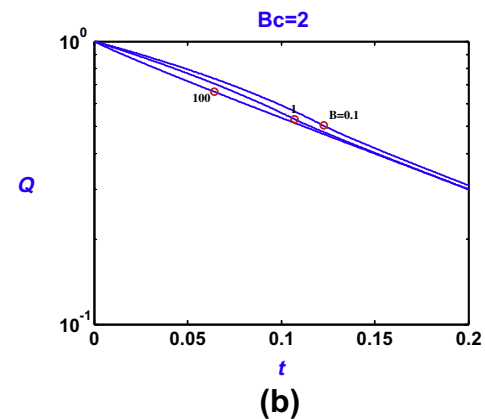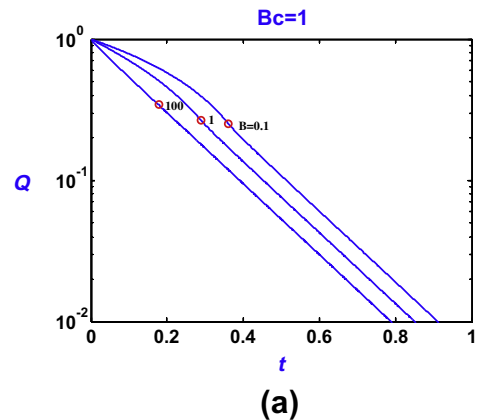
Fig. 8. Evolution of the volumetric flow rate in cessation of axisymmetric Newtonian Poiseuille flow for $s = 1$ and various values of the slip number: (a) $B_c = 1$; (b) $B_c = 2$; and (c) $B_c = 3$. The circles correspond to t_c (cessation of slip).

Fig. 7. The critical time for the cessation of wall slip t_c in cessation of axisymmetric Newtonain Poiseuille flow for various values of the slip yield stress ($s = 1$). The dotted lines are the estimates obtained using only the leading term in the expression used to calculate t_c.

numerical experiments also showed that cessation becomes faster as the slip exponent s is reduced, especially in the initial stages of the flow. The influence of s becomes weaker when slip is strong (i.e. as B is reduced).

5. Numerical results

The time-dependent viscoplastic flow is solved numerically, since it is not amenable to analytical solution. The non-dimensionalized version of the regularized Herschel–Bulkley Eq. (5) is

$$\tau_{rz} = \left\{ \frac{Bn[1 - \exp(-M\,\dot{\gamma})]}{\dot{\gamma}} + \dot{\gamma}^{n-1} \right\} \frac{\partial u_z}{\partial r} \qquad (46)$$

where $\dot{\gamma} = |\partial u_z/\partial r|$, while the stress growth exponent M is given by

$$M \equiv \frac{mV}{H} \qquad (47)$$

We used 100 quadratic finite elements in space and finite differences in time. For the time discretization, we used the standard fully implicit Euler backward-difference scheme with a dimensionless time step $\Delta t \leqslant 10^{-4}$. The criteria for convergence of the system of equations were that the norm of the error for the velocities and the norm of the residuals were both less than 10^{-4}. The effect of M in cessation of plane Couette and Poiseuille flows with no-slip at the wall was studied and discussed by Chatzimina and co-workers [10,16]. They noted in particular that when the imposed pressure is non-zero but below the critical value for the occurrence of steady Poiseuille flow, regularized flow reaches a steady-state corresponding to a small volumetric flow rate (the value of which decreases with M) while ideal Bingham flow ceases at a finite time. In the present work the imposed pressure gradient is zero in all cases.
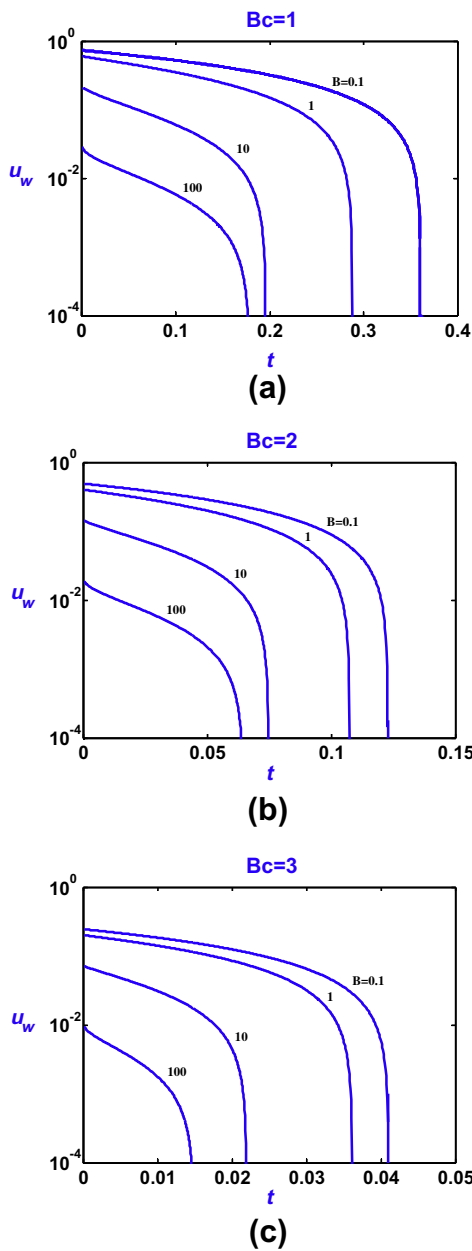
Fig. 9. Evolution of the slip velocity in cessation of axisymmetric Newtonian Poiseuille flow for $s = 1$ and various values of the slip number: (a) $B_c = 1$; (b) $B_c = 2$; and (c) $B_c = 3$.
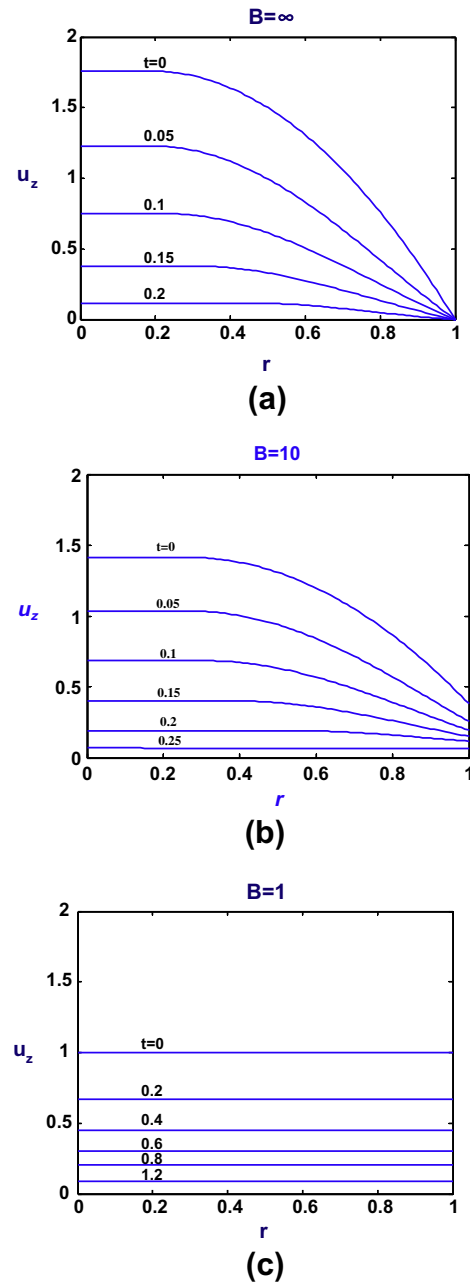
Fig. 10. Evolution of the velocity in cessation flow of a Bingham plastic with $Bn = 1$, $s = 1$ and zero slip yield stress ($B_c = 0$): (a) $B = \infty$ (no slip); (b) $B = 5$; and (c) $B = 1$ (plug flow).

Unless otherwise indicated, the results of this section have been obtained with $M = 1000$.

5.1. Results for zero slip yield stress

The numerical simulations of the cessation flow show that the velocity becomes and remains uniform before complete cessation. The evolution of the velocity for $s = 1$, $Bn = 1$, and various slip numbers, i.e., $B = \infty$ (no slip), $B = 5$ (strong slip), and $B = 1$ (full slip, since the critical slip number for attaining a uniform steady-state velocity profile in axisymmetric Poiseuille flow is $B_{crit} = Bn - B_c$), is illustrated in Fig. 10. Obviously, as the slip number is increased, the initial velocity profile becomes more flat and a uniform profile is attained earlier during cessation. Fig. 11 shows the evolution of
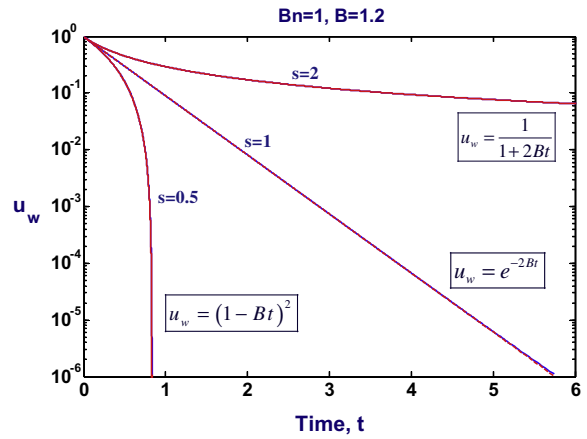

Fig. 12. Evolution of the slip velocity in cessation flow of a Bingham plastic with $Bn = 1$, $B = 1.2$, and zero slip yield stress ($B_c = 0$): (a) $s = 0.5$; (b) $s = 1$; and (c) $s = 2$. The predictions of Eq. (49) for $s = 1$ and (50) for $s = 0.5$ and 2, with $u_{w0} = 1$ and $t_0 = 0$ essentially coincide with the numerical solution.
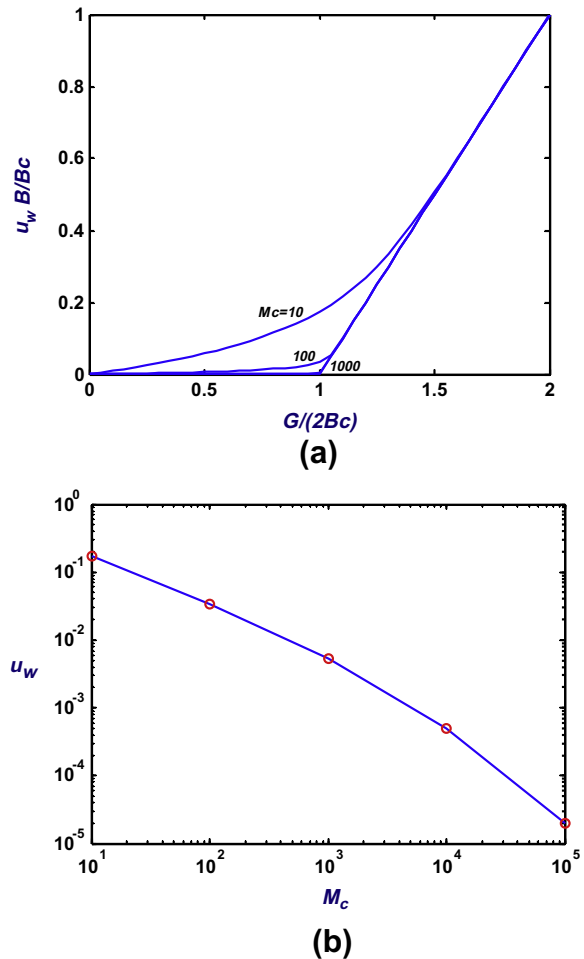

Fig. 11. Evolution of the volumetric flow rate in cessation flow of a Bingham plastic with $Bn = 1$, zero slip yield stress ($B_c = 0$) and various slip numbers: (a) $s = 0.5$; (b) $s = 1$; and (c) $s = 2$.

Fig. 13. Effect of the regularization parameter on the calculated solution: (a) slip velocity as a function of the imposed pressure gradient; (b) slip velocity at the critical pressure gradient $G/(2B_c)$; Newtonian flow with $B = B_c = s = 1$.

the volumetric flow rate Q for $Bn = 1$ and different slip numbers for three representative values of the slip exponent s: 0.5, 1, and 2. One observes that the stopping time is finite only in the case of no slip ($B \to \infty$) when $s < 1$. When s is fixed, the stopping time
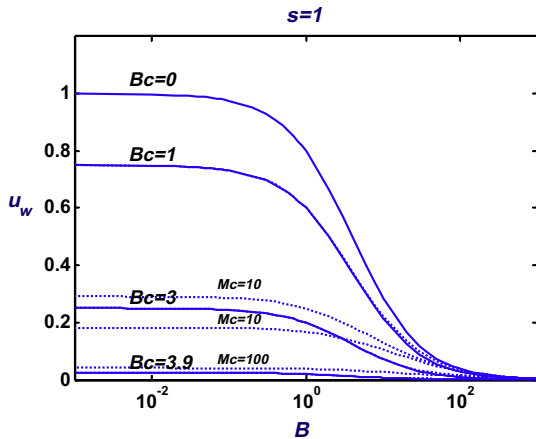
Fig. 14. Calculated slip velocities for various slip yield stress numbers B_c compared to the theoretical solution. In all cases, the numerical predictions for M_c = 10, 100, and 1000 are plotted with dotted lines. Newtonian flow with s = 1.

increases with the slip coefficient. In the case of Navier slip (s = 1), the stopping time is infinite for any non-zero Bingham number and the volumetric flow rate decays exponentially. When $s > 1$, the decay is much slower.

An (approximate) analytical solution can be obtained in the limiting case the velocity becomes uniform everywhere, except in a very thin zone adjacent to the wall, so that the wall shear stress is non-zero and the slip equation is satisfied. This situation also appears in steady flow, in regime (iv) of Fig. 2. The flow is entirely due to wall slip and there is no shear flow within the bulk where the velocity is flat except for a sharp discontinuity very close to the wall. Let t_0 denote the critical time at which the velocity becomes uniform, i.e. $u_z = u_w(t_0) = u_{w0}$. Integrating the momentum equation over the tube cross-section leads to the following ODE:

$$\frac{du_w}{dt} = -2\tau_w = -2Bu_w^s \tag{48}$$

Therefore, when s = 1, the velocity decays exponentially:

$$u_z = u_{w0} \exp[-2B(t - t_0)], \quad t \geqslant t_c \tag{49}$$

where $u_{w0} = u_w(t_0)$. Otherwise,

$$u_z = \left[u_{w0}^{1-s} - 2(1-s)B(t-t_0)\right]^{1/(1-s)}, \quad t \geqslant t_0 \tag{50}$$
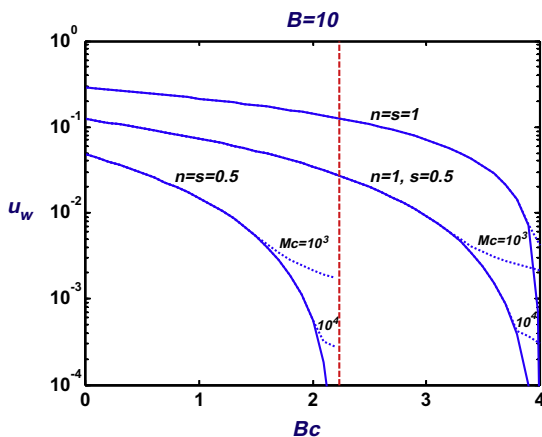

Fig. 15. Calculated slip velocities as functions of the slip yield stress for B = 10 and different combinations of n and s and M_c = 1000 and 10000. The solid lines correspond to the theoretical estimates. The vertical line corresponds to $B_{c,max} = \sqrt{5}$ for n = 0.5

Hence the stopping time is finite only if $s < 1$, in which case

$$t_s = t_0 + \frac{u_{w0}^{1-s}}{2(1-s)B} \tag{51}$$

In Fig. 12, the slip velocities predicted using Eqs. (49) and (50) are compared to the numerical solutions taking Bn = 1 and B = 1.2, considering three different values for s (0.5, 1, and 2), and assuming that u_{wc} = 1 and t_c = 0. Given that B is close to Bn, the numerical results practically coincide with the theoretical estimates.

5.2. Results for non-zero slip yield stress

In order to avoid the difficulties posed by the discontinuity of slip Eq. (17), we regularize it as follows:

$$\tau_w = B_c[1 - \exp(-M_c u_w)] + Bu_w^s \tag{52}$$
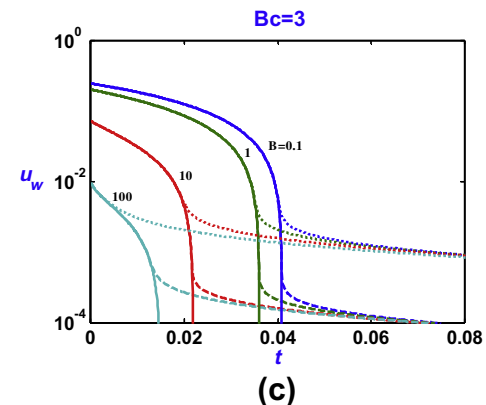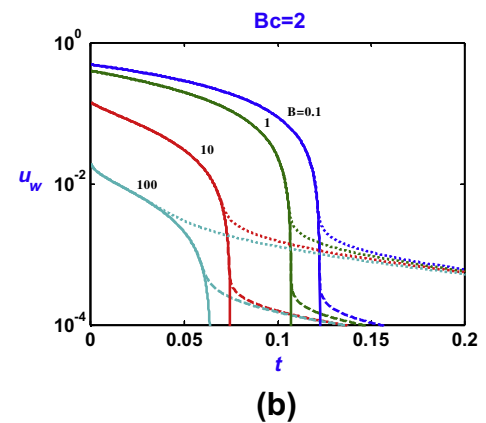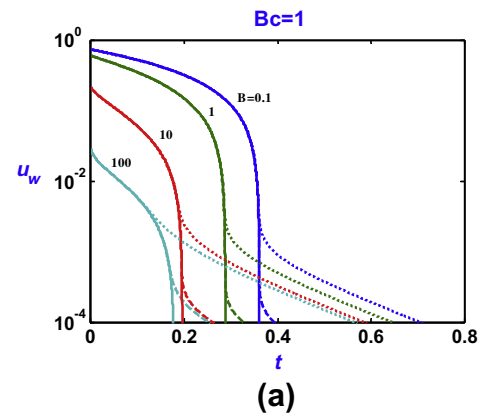

(a)

(b)

(c)

Fig. 16. Computed slip velocities in cessation of axisymmetric Newtonian Poiseuille flow for various values of the slip number and M_c = 1000 (dotted), 10,000 (dashed), and 100,000 (solid): (a) B_c = 1; (b) B_c = 2; and (c) B_c = 3.

where $M_c \equiv m_c V$ is a dimensionless growth parameter similar to the stress growth exponent of the Papanastasiou equation. For sufficiently large values of M_c, Eq. (52) provides a good approximation of Eq. (17). To illustrate this, let us first consider the steady-state Newtonian flow with $B = B_c = s = 1$. From Eq. (21), we observe that

$$\frac{u_w B}{B_c} = \begin{cases} 0, & G \leqslant 2B_c \\ \frac{G}{2B_c} - 1, & G > 2B_c \end{cases} \qquad (53)$$

In Fig. 13a, we compare the numerical solutions obtained for various values of M_c against Eq. (53). It should be noted that this particular plot has been constructed by specifying the pressure gradient G (and not the volumetric flow rate). We observe that for very high values of M_c, the numerical solution approaches theory very well. This is also illustrated in Fig. 13b, where the numerical steady-state

slip velocity for $G/(2B_c) = 1$ is plotted as a function of M_c. For $M_c \approx 50,000$, this velocity is smaller than the tolerance used for the finite element calculations.

The calculated steady-state slip velocities for various slip yield stress numbers B_c are compared to the theoretical solution in Fig. 14. In all cases, the numerical predictions for $M_c = 10$, 100, and 1000 are plotted with dotted lines. We observe that small values of M_c may be used only for moderate values of B_c. Higher values are required at higher values of B_c and/or B, i.e. when slip is weak. The validity of the regularized slip equation has also been tested for different values of the exponents n and s and in time-dependent calculations. In Fig. 15, the numerical predictions of the slip velocity for $B = 10$, obtained with $Mc = 1000$ and 10,000 are compared against analytical solutions provided in Table 1. The agreement is very close when slip is strong. As B_c approaches $B_{c,\,max}$, i.e. when slip is weak, higher values of M_c are needed in order to obtain accurate results.
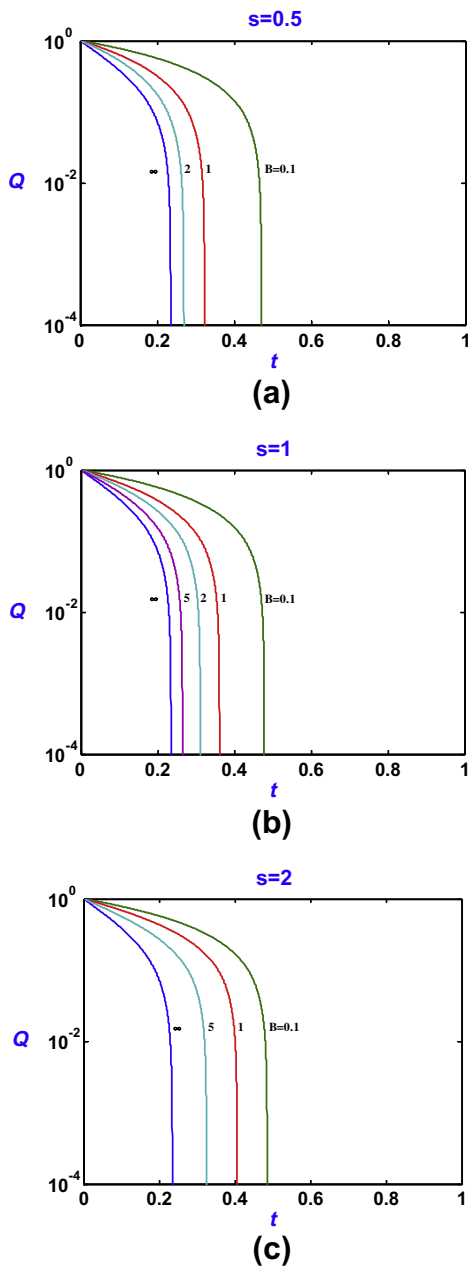

Fig. 17. Evolution of the volumetric flow rate in cessation of axisymmetric Poiseuille flow of a Bingham fluid for $Bn = B_c = 1$ and various slip numbers: (a) $s = 0.5$; (b) $s = 1$; and (c) $s = 2$. $M_c = 100000$.
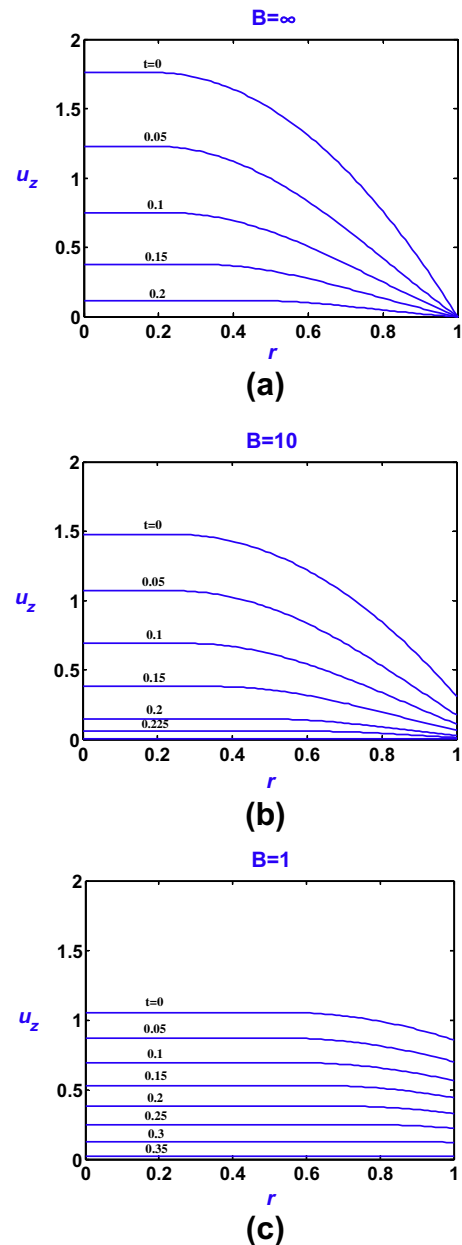

Fig. 18. Evolution of the volumetric flow rate in cessation flow of a Bingham plastic with $Bn = B_c = 1$, and $s = 1$: (a) $B = \infty$ (no slip); (b) $B = 10$; and (c) $B = 1$.

The effect of the regularization parameter M_c becomes more important in time-dependent calculations. Fig. 16 shows the evolution of the slip velocity for B_c = 1, 2, and 3 and different values of B and M_c. One observes that if M_c is not sufficiently large, the slip velocity does not vanish abruptly but it goes to zero asymptotically, after an initial quick decrease. The choice M_c = 10,000 ensures that the error in the numerical slip velocity is less than the tolerance used for the convergence of the Newton method and leads to stopping times of acceptable accuracy.

To investigate the effect of slip yield stress, we assumed that $Bn = B_c$, so that the initial velocity profile corresponds to case (ii) of Fig. 2. The evolution of the volumetric flow rate for $Bn = B_c = 1$ is illustrated in Fig. 17 for different values of s and B. The evolution of the velocity profile for the above choice of Bn and B_c, $s = 1$, and different values of the slip number is illustrated in Fig. 18. As expected, with non-zero slip yield stress the flow of a Bingham fluid stops at a finite time. A lower bound for the stopping time is obviously the bound derived by Glowinski [2] for the no-slip flow. The stopping time increases with slip (i.e., as B is reduced) and the value of the exponent s. Our calculations showed that as the value of the slip yield stress increases towards the limiting value $B_{c,\ max} = 4$, the effect of the slip number becomes less pronounced and the solution approaches that corresponding to no slip, as expected.

6. Conclusions

We studied the cessation of axisymmetric Poiseuille flow of a Herschel–Bulkley fluid with wall slip following a static slip law with slip yield stress. For the numerical simulations both the constitutive and slip equations have been regularized. The numerical calculations showed that when slip yield stress is zero, the fluid slips at the wall at all times, the velocity becomes and remains uniform before complete cessation, and the stopping time is finite only when the slip exponent is less than unity. When the slip yield stress is non-zero, slip ceases at a finite critical time, the velocity becomes flat only at complete cessation, and the stopping time is finite in all cases. As noted by Hatzikiriakos [24] static slip models are not valid in transient flows, since slip relaxation effects might become important, leading to delayed slip and other phenomena. We are currently investigating the use of dynamic slip models in transient Newtonian and non-Newtonian flows. The performance of the regularized slip equation in two-dimensional flow problems, in which the parts of the boundary along which slip occurs or not are unknown, is also a subject of our current research.

Acknowledgments

References

[1] T. Papanastasiou, G. Georgiou, A. Alexandrou, Viscous Fluid Flow, CRC Press, Boca Raton, 2000.
[2] R. Glowinski, Numerical Methods for Nonlinear Variational Problems, Springer-Verlag, New York, 1984.
[3] R.R. Huilgol, B. Mena, J.-M. Piau, Finite stopping time problems and rheometry of Bingham fluids, J. Non-Newtonian Fluid Mech. 102 (2002) 97.
[4] Q.D. Nguyen, D.V. Boger, Measuring the flow properties of yield stress fluids, Annu. Rev. Fluid Mech. 24 (1992) 47.
[5] V. Bertola, F. Bertrand, H. Tabuteau, D. Bonn, P. Coussot, Wall slip and yielding in pasty materials, J. Rheol. 47 (2003) 1211.
[6] Coussot, L. Tocquer, C. Lanos, G. Ovarlez, Macroscopic vs. local rheology of yield stress fluids, J. Non-Newtonian Fluid Mech. 158 (2009) 85.
[7] T.C. Papanastasiou, Flows of materials with yield, J. Rheol. 31 (1987) 385.
[8] G.R. Burgos, A.N. Alexandrou, V. Entov, On the determination of yield surfaces in Herschel–Bulkley fluids, J. Rheol. 43 (1999) 463.
[9] Y. Dimakopoulos, J. Tsamopoulos, Transient displacement of a viscoplastic material by air in straight and suddenly constricted tubes, J. Non-Newtonian Fluid Mech. 112 (2003) 43.
[10] M. Chatzimina, G. Georgiou, I. Argyropaidas, E. Mitsoulis, R.R. Huilgol, Cessation of Couette and Poiseuille flows of a Bingham plastic and finite stopping times, J. Non-Newtonian Fluid Mech. 129 (2005) 117.
[11] I.A. Frigaard, C. Nouar, On the usage of viscosity regularization methods for viscoplastic fluid flow computation, J. non-Newtonian Fluid Mech. 127 (2005) 1.
[12] L. Muravleva, E. Muravleva, G.C. Georgiou, E. Mitsoulis, Numerical simulations of cessation flows of a Bingham plastic with the Augmented Lagrangian Method, J. Non-Newtonian Fluid Mech. 165 (2010) 544.
[13] L. Muravleva, E. Muravleva, G.C. Georgiou, E. Mitsoulis, Unsteady circular Couette flow of a Bingham plastic with the Augmented Lagrangian Method, Rheol. Acta 49 (2010) 1197.
[14] E.J. Dean, R. Glowinski, G. Guidoboni, On the numerical simulation of Bingham visco-plastic flow: old and new results, J. Non-Newtonian Fluid Mech. 142 (2007) 36.
[15] R.R. Huilgol, Variational inequalities in the flows of yield stress fluids including inertia: theory and applications, Phys. Fluids 14 (2002) 1269.
[16] M. Chatzimina, C. Xenophontos, G. Georgiou, I. Argyropaidas, E. Mitsoulis, Cessation of annular Poiseuille flows of Bingham plastics, J. Non-Newtonian Fluid Mech. 142 (2007) 135.
[17] H. Zhu, D. De Kee, A numerical study for the cessation of Couette flow of non-Newtonian fluids with a yield stress, J. Non-Newtonian Fluid Mech. 143 (2007) 64.
[18] U. Yilmazer, D.M. Kalyon, Slip effects in capillary and parallel disk torsional flows of highly filled suspensions, J. Rheol. 33 (1989) 1197.
[19] H.A. Barnes, A review of the slip (wall depletion) of polymer solutions, emulsions and particle suspensions in viscometers: its cause, character, and cure, J. Non-Newtonian Fluid Mech. 56 (1995) 221.
[20] P. Ballesta, G. Petekidis, L. Isa, W.C.K. Poon, R. Besseling, Wall slip and flow of concentrated hard-sphere colloidal suspensions, J. Rheol. 56 (2012) 1005.
[21] M.M. Denn, Extrusion instabilities and wall slip, Ann. Rev. Fluid Mech. 33 (2001) 265.
[22] D.M. Kalyon, Apparent slip and viscoplasticity of concentrated suspensions, J. Rheol. 49 (2005) 621.
[23] C.L.M.H. Navier, Sur les lois du mouvement des fluides, Mem. Acad. R. Sci. Inst. Fr. 6 (1827) 389.
[24] S.G. Hatzikiriakos, Wall slip of molten polymers, Progr. Polym. Sci. 37 (2012) 624.
[25] Y. Damianou, G.C. Georgiou, I. Moulitsas, Combined effects of compressibility and slip in flows of a Herschel–Bulkley fluid, J. Non-Newtonian Fluid Mech. 193 (2013) 89.
[26] Y. Cohen, A.B. Metzner, Apparent slip of polymer solutions, J. Rheol. 29 (1985) 67.
[27] T.Q. Jiang, A.C. Young, A.B. Metzner, The rheological characterization of HPG gels: measurement of slip velocities in capillary tubes, Rheol. Acta 25 (1986) 397.
[28] H.C. Lau, W.R. Schowalter, A model of adhesive failure of viscoelastic fluids during flow, J. Rheol. 30 (1996) 193.
[29] D.A. Hill, T. Hasegawa, M.M. Denn, On the apparent relation between the adhesive failure and melt fracture, J. Rheol. 34 (1990) 891.
[30] S.G. Hatzikiriakos, J.M. Dealy, Wall slip of molten high density polyethylenes. II. Capillary rheometer studies, J. Rheol. 36 (1992) 703.
[31] G. Hay, M.E. Mackay, S.A. McGlashan, Y. Park, Comparison of shear stress and wall slip measurement techniques on a linear low density polyethylene, J. Non-Newtonian Fluid Mech. 92 (2000) 187.
[32] J. Pérez-González, J.J. López-Durán, B.M. Marín-Santibáñez, F. Rodriguez-González, Rheo-PIV of a yield-stress fluid in a capillary with slip at the wall, Rheol. Acta 51 (2012) 937.
[33] H. Spikes, S. Granick, Equation for slip of simple liquids at smooth solid surfaces, Langmuir 19 (2003) 5065.
[34] A.V. Ramamurthy, Wall slip in viscous fluids and influence of materials of construction, J. Rheol. 30 (1986) 337.
[35] D.S. Kalika, M.M. Denn, Wall slip and extrudate distortion in linear low-density polyethylene, J. Rheol. 31 (1987) 815.
[36] S.G. Hatzikiriakos, J.M. Dealy, Wall slip of molten high density polyethylene. I. Sliding plate rheometer studies, J. Rheol. 35 (1991) 497.
[37] D.M. Kalyon, H. Gevgilili, Wall slip and extrudate distortion of three polymer melts, J. Rheol. 47 (2003) 683.
[38] F. Brochard-Wyart, P.G. de Gennes, Shear-dependent slippage at a polymer/solid interface, Langmuir 8 (1992) 3033.
[39] T. Sochi, Slip at fluid-solid interface, Polym. Rev. 51 (2011) 309.
[40] P.A. Durbin, Considerations on the moving contact-line singularity, with application to frictional drag on a slender drop, J. Fluid Mech. 197 (1988) 157.
[41] C. Le Roux, A. Tani, Steady solutions of the Navier–Stokes equations with threshold slip boundary conditions, Math. Methods Appl. Sci. 30 (2007) 595.
[42] J.M. Piau, Carbopol gels: elastoviscoplastic and slippery glasses made of individual swollen sponges: meso- and macroscopic properties, constitutive equations and scaling laws, J. Non-Newtonian Fluid Mech. 144 (2007) 1.
[43] N. Roquet, P. Saramito, An adaptive finite element method for viscoplastic flows in a square pipe with stick-slip at the wall, J. Non-Newtonian Fluid Mech. 155 (2008) 101.
[44] A. Fortin, D. Côté, P.A. Tanguy, On the imposition of friction boundary conditions for the numerical simulation of Bingham fluid flows, Comp. Methods Appl. Mech. Eng. 88 (1991) 97.

[45] S.G. Hatzikiriakos, I.G. Kazatchkov, Interfacial phenomena in the capillary extrusion of metallocene polyethylenes, J. Rheol. 41 (1997) 1299.

[46] J.R. Seth, M. Cloitre, R.T. Bonnecaze, Influence of short-range forces on wall-slip in microgel pastes, J. Rheol. 52 (2008) 1241.

[47] J.H. Choo, R.P. Glovnea, A.K. Forest, H.A. Spikes, A low friction bearing based on liquid slip at the wall, ASME J. Tribol. 129 (2007) 611.

[48] P. Ballesta, R. Besseling, L. Isa, G. Petekidis, W.C.K. Poon, Slip and flow of hard-sphere colloidal glasses, Phys. Rev. Let. 101 (2008) 258301.

[49] S.G. Hatzikiriakos, A slip model for linear polymers based on adhesive failure, Intern. Polym. Process. 8 (1993) 135.

[50] J.M. Piau, N. El Kissi, Measurement and modelling of friction in polymer melts during macroscopic slip at the wall, J. Non-Newtonian Fluid Mech. 54 (1994) 121.

[51] A.I. Leonov, On the dependence of friction force on sliding velocity in the theory of adhesive friction of elastomers, Wear 141 (1990) 137.

[52] H.S. Tang, D.M. Kalyon, Unsteady circular tube flow of compressible polymeric liquids subject to pressure-dependent wall slip, J. Rheol. 52 (2008) 507.

[53] H.S. Tang, D.M. Kalyon, Time-dependent tube flow of compressible suspensions subject to pressure dependent wall slip: ramifications on development of flow instabilities, J. Rheol. 52 (2008) 1069.

[54] J.R.A. Pearson, C.J.S. Petrie, On the melt-flow instability of extruded polymers, Proc. 4th Int. Rheol. Congr. 3 (1965) 265.

[55] C. Métivier, A. Magnin, The effect of wall slip on the stability of the Rayleigh–Bénard Poiseuille flow of viscoplastic fluids, J. Non-Newtonian Fluid Mech. 166 (2011) 839.

[56] S.P. Meeker, R.T. Bonnecaze, M. Cloitre, Slip and flow in pastes of soft particles: direct observation and rheology, J. Rheol. 48 (2004) 1295.

[57] R.R. Huilgol, Variational principles and variational inequality for a yield stress fluid in the presence of slip, J. Non-Newtonian Fluid Mech. 75 (1998) 231.

[58] H.A. Spikes, The half-wetted bearing. Part 1: Extended Reynolds equation, Proc. Inst. Mech. Eng., Part J: J. Eng. Trib. 217 (2003) 1.

[59] M. Tauviqirrahman, R. Ismail, J. Jamari, D.J. Schipper, A study of surface texturing and boundary slip on improving the load support of lubricated parallel sliding contacts, Acta Mech. 224 (2013) 365.

[60] G. Kaoullas, G.C. Georgiou, Newtonian Poiseuille flows with wall slip and non-zero slip yield stress, J. Non-Newtonian Fluid Mech. 197 (2013) 24.

[61] G.C. Georgiou, G. Kaoullas, Newtonian flow in a triangular duct with slip at the wall, Meccanica (2013), http://dx.doi.org/10.1007/s11012-013-9787-7 (in press).

[62] G. Kaoullas, G.C. Georgiou, Slip yield stress effects in start-up Newtonian Poiseuille flows, Rheol. Acta 52 (2013) 913.

[63] D.M. Kalyon, P. Yaras, B. Aral, U. Yilmazer, Rheological behavior of a concentrated suspension: a solid rocket fuel stimulant, J. Rheol. 37 (1993) 35.

[64] A. Lindner, P. Coussot, D. Bonn, Viscous fingering in a yield stress fluid, Phys. Rev. Let. 85 (2000) 314.